NIST Technical Note XXXX

Flow resistance through vegetative

Ryan Falkenstein-Smith
Kevin McGrattan
Marco Fernandez

This publication is available free of charge from:
https://doi.org/10.6028/NIST.TN.XXXX

National Institute of
Standards and Technology
U.S. Department of Commerce

NIST Technical Note XXXX

Flow resistance through vegetative

Ryan Falkenstein-Smith
Kevin McGrattan
Marco Fernandez
Fire Research Division
Engineering Laboratory

This publication is available free of charge from:
https://doi.org/10.6028/NIST.TN.XXXX

Month Year

U.S. Department of Commerce
Wilbur L. Ross, Jr., Secretary

National Institute of Standards and Technology
Walter Copan, NIST Director and Undersecretary of Commerce for Standards and Technology

National Institute of Standards and Technology Technical Note XXXX
Natl. Inst. Stand. Technol. Tech. Note XXXX, 14 pages (Month Year)
CODEN: NTNOEF

This publication is available free of charge from:
https://doi.org/10.6028/NIST.TN.XXXX

Abstract

This report documents a series of experiments carried out on a variety of vegetation canopy to determine their resistance to airflow. The objective of each experiment was a follows: Experiment 1) determine the vegetations' projected area using standard photography equipment and image analysis software, Experiment 2) measure the pressure loss across vegetation canopy while exposed to steady wind speeds in an open circuit wind tunnel, and Experiment 3) quantify the total volume of the vegetation canopy using a water displacement technique. The results obtained from these experiments were combined to calculate the drag coefficient of the vegetation canopy and provided further insight into the relationship between the vegetations' geometric properties and resistance to airflow. Furthermore, specific parameters determined from the experiments were incorporated into well-established hydraulic resistance models of configurations with similar geometry (i.e., tube banks) to validate the calculated drag coefficients of the vegetation canopy.

Key words

Vegetation Canopy; Drag Coefficient; Wind Tunnel; Tube Banks.

Table of Contents

List of Tables

List of Figures

1. Introduction

The rise in wildfires across the United States presents a substantial risk for the destruction of communities residing in wildland-urban interfaces. According to the Insurance Information Institute [1], approximately 10 million acres within the United States were burned last year; up 4.6 million from the previous year. One tool that could substaintially mitigate the structural losses caused by wildfires is the use of numerical simulations. More specifically, numerical simulations can be used to predict the fire propagation throughout different types of wild terrain which would aid in the containment, reduction, and extinction of wildfires.

One crucial component to fire behavior prediction is the use of an accurate wind-driven flow around and within vegetation residing in wildlands. In this report, vegetation refers primarily to the canopy of a plant (i.e., branches and foliage). Most vegetation exhibits a complex porous structure that is unevenly distributed and asymmetric. As a consequence of vegetation's complicated geometry, it is difficult to establish flow characteristics within the vegetation. The experiments described in this report are intended to establish geometric features that can be used to determine the drag coefficient of vegetation.

1.1 Flow Through Vegetation

Compared to solid objects with simple geometries, vegetation can improve momentum absorption due to its porosity and multi-component configuration. The internal spacings encompassed by leaves and branches provides the vegetation with a higher surface area, allowing more fluid energy to dissipate as the flow moves through the vegetation. Since vegetation can be treated as a multi-component element, the total drag force (F_D [N]) representing the momentum transferred from the fluid to a collection of components within the vegetation is obtained from the summation of each component per unit volume (Eq. 1). In a simplified model, the multi-component strucutre of vegetation can be adapted into a collection of cylindrical particles, similar to the geometric configuration of a tube bank (Fig. 1).

$$F_D = \frac{1}{V}\Sigma\left[\frac{1}{2}\rho C_D A_p U^2\right] \tag{1}$$

In the equation above, A_p is projected area of the element (m^2), ρ is the air density ($kg\,m^{-3}$), U is the free stream velocity ($m\,s^{-1}$), and C_D is the drag coefficient. Similar configurations have already been been adapted in numerical simulation investigations [2, 3] in which certain geometric features are assumed to understand flow characteristics through vegetation. Other numerical simulation studies [4] have expanded upon Eq. 1 by including additional parameters such as shape factor (C_S), solid fraction, (β), and surface to volume ratio ($\sigma[m^{-1}]$). The expanded equation could then be used to better characterize the relationship between flow and vegetation geometric features and resulting in Eq. 2.

$$F_D = \frac{1}{2}\rho C_D C_s \beta \sigma U^2 \tag{2}$$

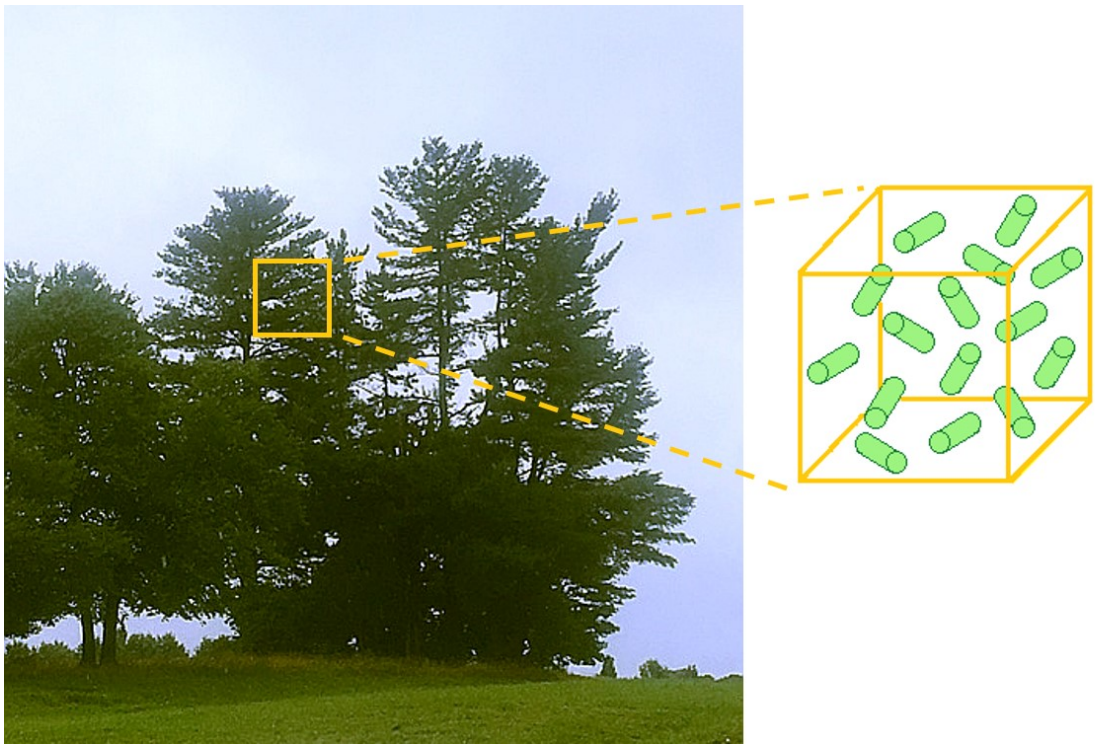

Fig. 1. Vegetation translation to multi-component model

Note that Eq. 2 is a volumetric force that is directly related to the differential pressure (ΔP) across the control volume by a distance (L [m]). Therefore the relationship between volumetric force and the fluid momentum can be rearranged in Eq. 2 to incorporate the pressure loss across the control volume (Eq. 3).

$$\Delta P = \frac{L}{2}\rho C_{\mathrm{D}} C_{\mathrm{s}} \beta \sigma U^2 \tag{3}$$

Some of the terms presented in Eq. 3 are challenging to experimentally quantify, such as the shape factor and surface to volume ratio. However, some of these terms (σ, β, and C_S) can be combined into a single parameter defined as the absorption coefficient ($\varkappa$). Here, the absorption coefficient represents the vegetation density (area per unit volume) and can be obtained by determining the projected area per occupied volume of space. In other words, if light were to be projected through the frontal plane of the vegetation, then the amount of light that passes completely through the enitre vegetation volume represents the unoccupied space of the vegetation, also defined as the free area fraction (W). The relationship of the free area fraction and the absorption coefficient can be defined in Eq. 4 assuming that the array of light moving through the vegetation takes on an exponential function.

$$W = e^{-\kappa L} \tag{4}$$

where

$$\kappa = C_s \beta \sigma \tag{5}$$

1.2 Objective

The objective of the experiments described in this report is to quantify the resistance to flow for different vegetation configurations. Although there have been several experimental studies that determine the drag coefficient of entire plant structures [5–9], there has been little investigation on the resistance to flow exclusively through the vegetation canopy. In a more general sense, how does the flow resistance vary through the vegetation canopy? The exprements presented in this report attempt to adress this question to ultimately lay the foundation for accurate wind representation in numerical simulations.

2. Description of Experiments

2.1 Vegetation Preparation and Investigation Procedure

The vegetation chosen for this work was a Bakers Blue Spruce, an Evergreen Distylium, a Gold Rider Leyland Cypress , a Kimberley Queen Fern, a Blue Shag Eastern White Pine, and a Robin Red Holly. Each vegetation sample was chosen for this study based on their local availability. Leaf shapes of the vegetation samples included needle, elliptic, scale, and ovate shapes. To mimic a segment of vegetation canopy similarly investigated in a numerical simulation, samples were cut into 0.5 m x 0.5 m x 0.5 m cubes using a cubic guiding frame then to a thin steel plate (Fig. 2). The 0.5 m x 0.5 m cross-section of the segmented vegetation canopy fully occupied the cross-section of the wind tunnel forcing the flow to move through the vegetation as opposed to around it. The center of each cubic vegetation sample's side was marked on the base plate to better the perpendicular alignment of the vegetation to the flow when placed in the wind tunnel. To easily distinguish the front, back, left, and right side of the cube-shaped vegetation, each side was designated a name of position A (PA), position B (PB), position C (PC), or position D (PD) (Fig. 3). After its initial cut, image analysis, wind tunnel measurements, and water displacement testing were conducted in subsequent order. In some cases, additional cuts were made to certain samples at the conclusion of the experimental procedure (Fig. 4). The decision to make additional cuts made to the vegetation samples mainly depended on the lively hood of the particular sample after an iteration in the experimental procedure. In the case of the Bakers Blue Spruce, Gold Rider Leyland Cypress, and Robin Red Holly, four iterative cuts were made with the final cut being the removal of all leaves from the vegetation.

Fig. 2. Cutting procedure of vegetation samples

2.2 Image Analysis to Determine the Absorption Coefficient

The absorption coefficient of the vegetation samples were determined from the free area fraction (W) of the projected area of the sample. After segmenting the vegetation, the sample was placed on a table located between a large white backdrop and a 0.5 m x 0.5 m cardboard frame (Fig. 5). The cardboard frame dimensions were the same as cross-section dimensions within the wind tunnel, providing an accurate representation of the vegetation's

Fig. 3. Prepared vegetation sample's designated orientation

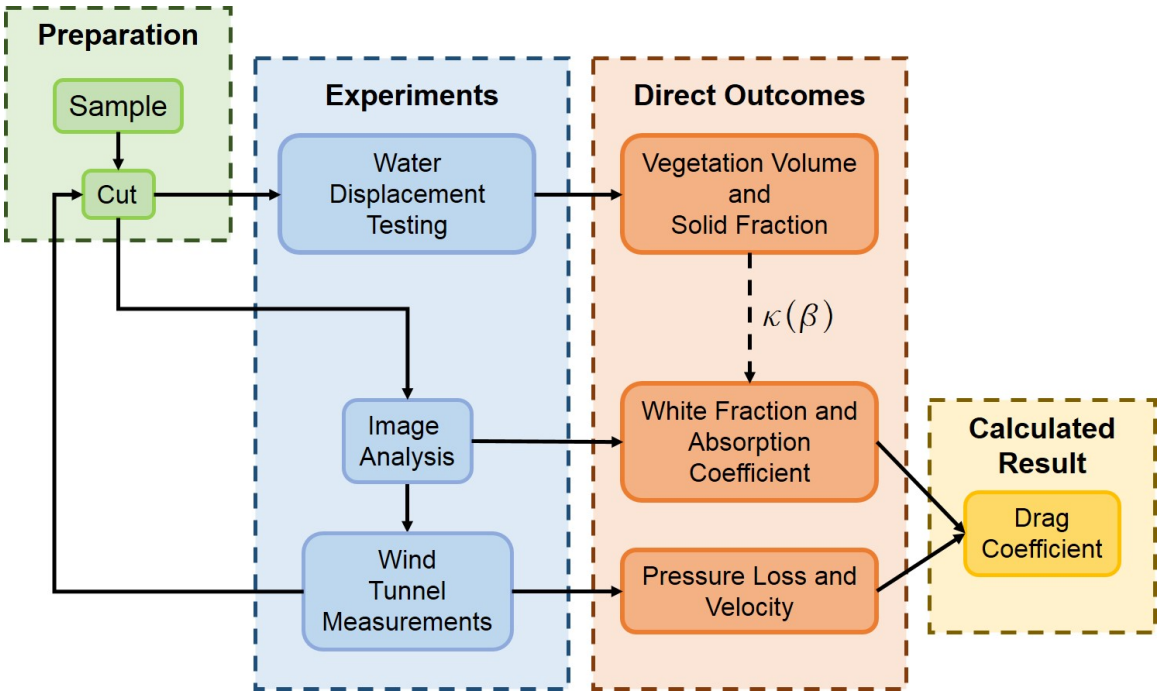

Fig. 4. Flowchart of experimental procedures and their respective outcomes

projected area when placed within the tunnel. For each sample cut, an image of each cubic sample's sides was captured. All images were captured using a Nikon D5600 camera placed on a tripod located approximately 3.6 m away from the frontal plane of the vegetation sample. In order to identify smaller areas of white space, the white backdrop was illuminated using a collection of incandescent and LED lights.

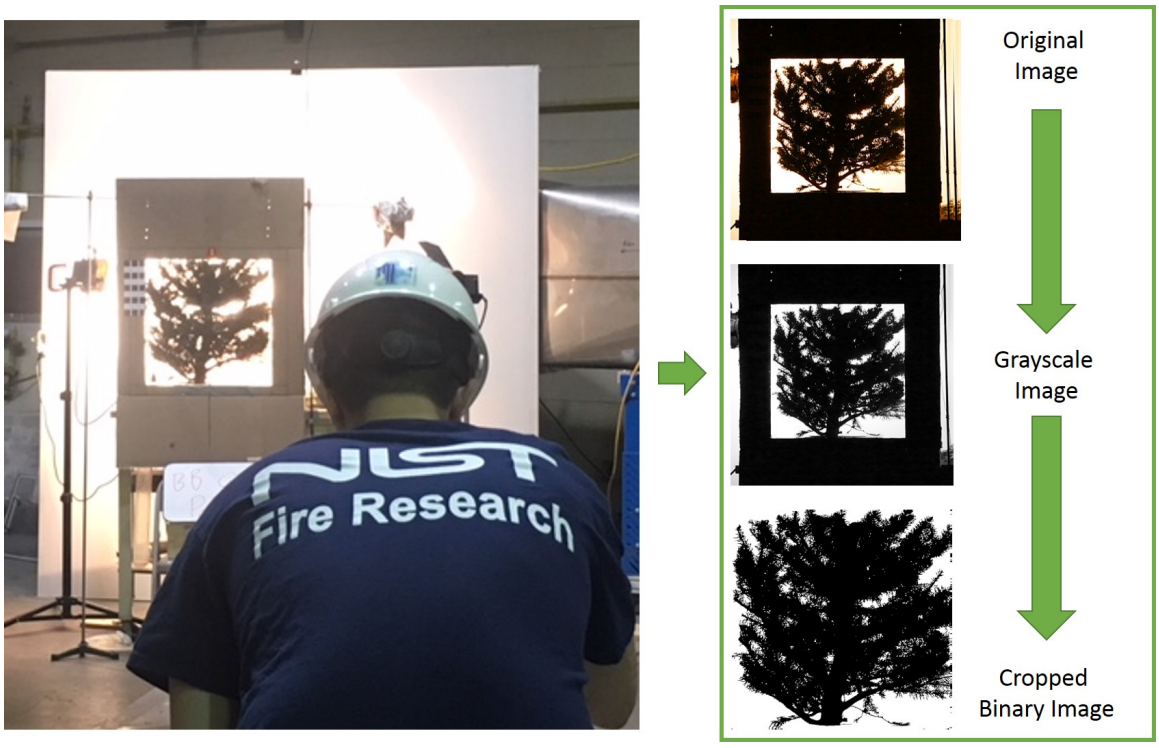

Fig. 5. Setup for photographing vegetation samples (left) and the post-processing procedure for analyzing images (right)

After photographing the projected area of vegetation, the captured images were processed using MATLAB's Image Processing Toolbox. Imported images were first cropped within the cardboard frame to eliminate nonvegetative substances and to exclusively evaluate the projected vegetation area. The obtained colored image was converted into a grey scale then binary (black and white) image using a pre-set threshold level. Once converted into a binary image, a pixel count was conducted to determine the free area fraction of the vegetation. After obtaining the free area fractions for each position of the vegetation sample, the average free area fraction was calculated by averaging the parallel sides of the cubic vegetation.

An uncertainty analysis was also conducted on the imaging process. Before using segmented vegetation samples, objects of known projected areas were photographed using the same imaging setup. It was found that with each object, the calculated free area fraction varied from the true value by 1%. Therefore, the error of the free area fraction values was

assumed to be 1%. The uncertainty of each determined free area fraction also accounted for the averaged value using propagation of error.

2.3 Wind Tunnel Experiments to Measure the Pressure Loss Across Vegetation

Pressure loss measurements were obtained in a wind tunnel test section with a cross-sectional area of 0.5 m x 0.5 m and a length of 2 m. Differential pressure was measured in two sections: 1) upstream using a Rosemont 485 Annubar Primary Element and 2) downstream between two pressure taps placed approximately 5 cm away from the vegetation sample (Fig. 6). The differential pressure was specifically measured using two MKS Baratron Type 220D Pressure Transducer with a range of 0 to 1 torr (133 Pa). The air flow was provided by a 0.91 m axial fan controlled by a variable frequency drive and monitored using the Annubar, which operates similar to pitot-static tube rake. Air density was calculated from the tunnel's internal temperature obtain from K-type thermocouple while also accounting for the pressure and humidity surrounding the wind tunnel. Each sample configuration was subjected to nine different fan speeds ranging from 0 to 88% of the full scale fan speed. The fan speed was not run at full scale due to the risk of exceeding the pressure tansducer's pressure limitations. During a wind tunnel test data was sampled at 90 Hz for a 30-second period while maintaining at a constant fan speed.

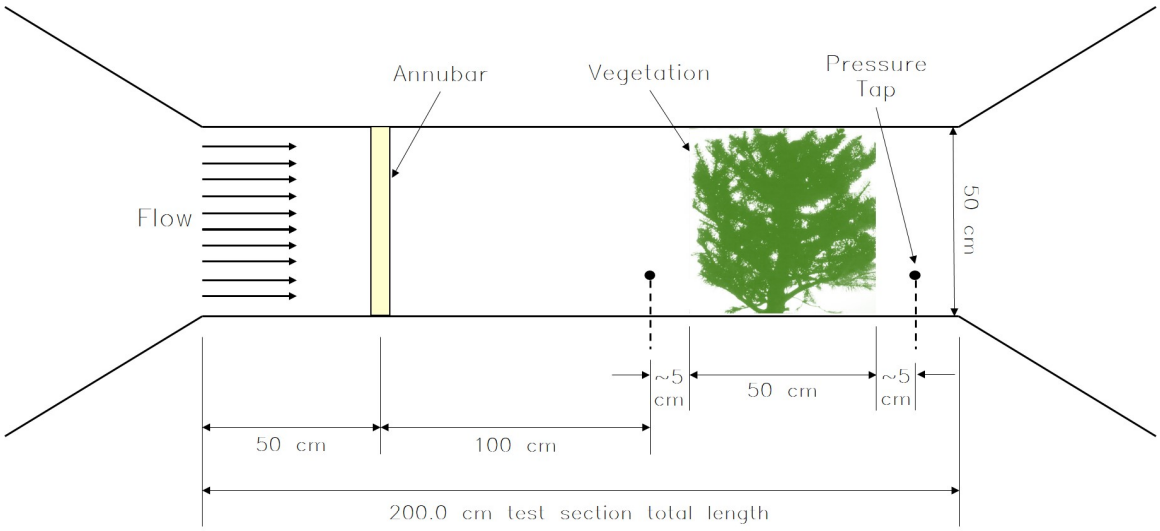

Fig. 6. Schematic diagram of the wind-tunnel experimental setup (not to scale)

Once a set of measurements were taken at all nine fan speeds, the wind tunnel was shut off for a short amount of time (approx. 5 min), then proceeded by a repeated test. All wind tunnel tests were repeated three times for each vegetation configuration. The variances of the repeated tests' datasets for a given sample, cut, and position were compared using Hartley's F_{Max} test. If it was found that the data sets were homogenous, then the data from

the repeated tests were pooled together and averaged within the corresponding 30-second sampling time.

An uncertainty analysis was also conducted for the wind tunnel measurements using propagation of error. The uncertainty of the pressure readings accounted for the calibration error (1.2 %) and the reported accuracy error (0.15% of the reading $\pm$ 0.02% of the reading per °C). The uncertainty of the air density was determined from the standard error of the sampling data. Since the velocity and subsequently calculated drag coefficient were functions of the pressure, density, and free area fraction measurements, their respective uncertainties were determined through propagation of error.

2.4 Water Displacement Testing to Determine the Volume and Solid Fraction (β)

The volume of vegetative solids was measured after a cut was made to the cubic vegetation sample. The remaining vegetative substance was separated into two groups of branches and leaves. Each group was packaged using a cloth mesh bag and thin wire. The wire volume and mass of the mesh bag and wire was measured before any displacement testing was conducted to determine only the vegetation material. Before submerging the packaged material, the dry weight of the sample was measured using a Mettler Toledo Jaguar load cell. After determining the dry weight, the packaged material was completely submerged in a bucket with a spout located approximately 3.8 cm from the top of the bucket. Before submerging the vegetation in water, the bucket was filled entirely with water, then allowed to drain at the lip of the spout to eliminate any additional displaced waterduring the test. Once the packaged vegetation was submerged, the displaced water was fed through the spout and into a glass beaker (Fig. 7). Testing concluded once the flow through tubing stopped or exhibited infrequent drips. The collected beaker water was then poured into a 1000 ml graduated cylinder to determine the volume of solid vegetation.

Fig. 7. Procedure of the water displacement test

Water displacement testing was conducted three times for each packaged vegetation. The weight of the vegetation was measured in between the displacement tests to account for any additional water that remained after the previous test. Once all volumes were determined for each vegetation cut, the solid fraction of the vegetation was calculated by

dividing by the occupied space of the vegetation sample (0.5 m x 0.5 m x 0.5 m = 0.125 m^3). The uncertainty of the measured volume and solid fraction were also calculated from the propagation of error using the resolution of the Mettler Toledo load cell (0.005 kg), the resolution of the graduated cylinder used to measure the volume of the displaced water (5 ml), and the variance of the repeated displacement tests.

3. Results

The key result of this work was the drag coefficient determined through a combination of the results provided from each experiment. Additionally, a relationship between the absorption coefficient and solid fraction was also obtained from the image analysis and water displacement experiments.

3.1 Vegetation Canopy Drag Coefficients

Table 1 shows the average drag coefficient, and its respective uncertainty of each vegetation configuration categorized by species, cut, and position.

Figure 8 shows the differential pressure measurements taken across the vegetation plotted against the free stream velocity. It can be observed that the differential pressure readings across a given velocity range are higher for vegetation configurations with higher free area fractions. By evaluating Eq. 3, the relationship between the dynamic pressure and the ratio between differential pressure measured across the vegetation and the product of the absorption coefficient and length can be seen in Fig. 9. Despite exhibiting different geometric characteristics, Fig. 9 demonstrates that by incorporating the absorption coefficient and length, the pressure ratio moderately collapses suggesting a fairly consistent drag coefficient for the variety of vegetation canopies.

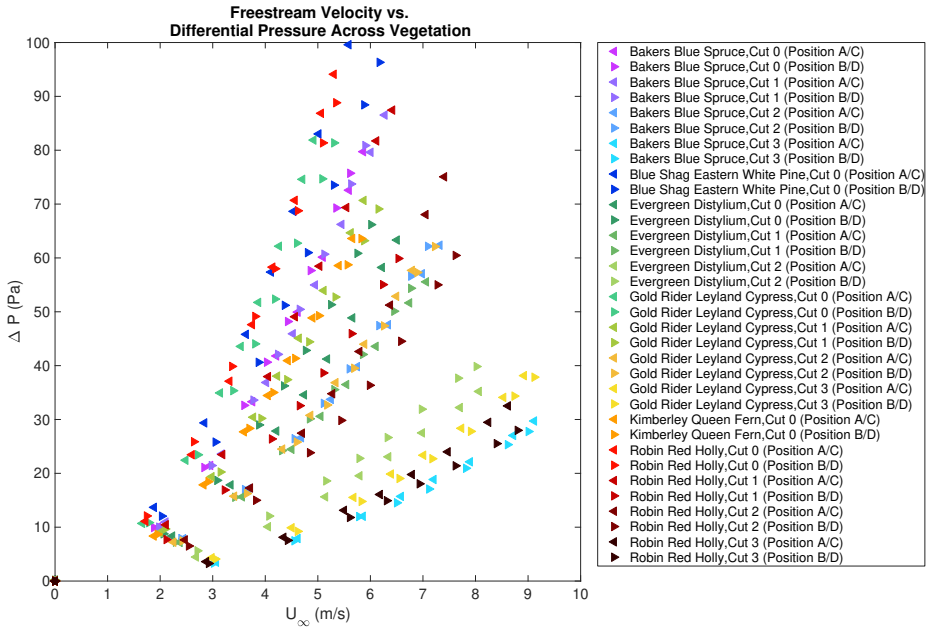

Fig. 8. Differential pressure measured across different vegetation samples subjected to various free stream velocities.

Table 1. Drag Coefficient Summary

Sample	Cut	Position	C_d	C_d Uncertainty
Bakers Blue Spruce	0	A/C	3.35	0.02
		B/D	3.10	0.01
	1	A/C	3.40	0.01
		B/D	3.29	0.02
	2	A/C	2.82	0.01
		B/D	2.74	0.01
	3	A/C	2.35	0.02
		B/D	2.26	0.01
Blue Shag Eastern White Pine	0	A/C	3.21	0.01
		/BD	3.14	0.01
Evergeen Distylium	0	A/C	3.15	0.01
		B/D	3.14	0.01
	1	A/C	2.87	0.01
		B/D	2.61	0.01
	2	A/C	1.85	0.01
		B/D	2.08	0.00
Gold Rider Leyland Cypress	0	A/C	3.18	0.01
		B/D	3.09	0.01
	1	A/C	3.29	0.01
		B/D	3.33	0.01
	2	A/C	2.57	0.01
		B/D	3.25	0.01
	3	A/C	2.97	0.01
		B/D	3.84	0.01
Kimberley Queen Fern	0	A/C	3.38	0.009
		B/D	2.82	0.007
Robin Red Holly	0	A/C	2.79	0.017
		B/D	2.66	0.005
	1	A/C	2.68	0.003
		B/D	1.91	0.006
	2	A/C	3.03	0.003
		B/D	2.34	0.011
	3	A/C	1.85	0.015
		B/D	1.64	0.012

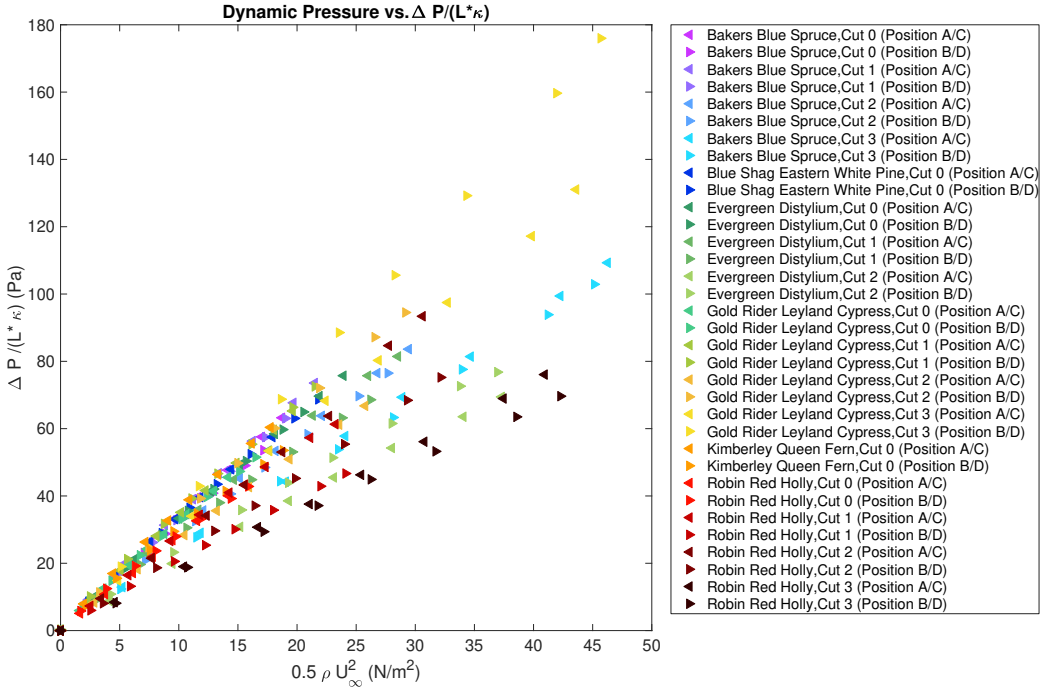

Fig. 9. Differential pressure across different vegetation samples over their respective ($\varkappa$L) vs. dynamic pressureof.

3.2 Relationship between the absorption coefficient ($\varkappa$) and solid fraction (β)

Figure 10 displays each samples' absorption coefficient plotted against their corresponding solid fractions. The markers presented in Figure 10 indicate the actual measured values while the dotted lines are a linear regression fit of the measured data. It can be observed that the absorption coefficient declines with the cut indicating that the removal of solid material from the vegetation after a cut increases the free area fraction, thus decreasing the absorption coefficient. Furthermore, Fig. 10 also shows a discrepancy between the sample positions of the same cut. The difference in the absorption coefficients suggests that the area distribution within the canopy structure is inhomogeneously distributed. In other words, the original assumption that the vegetation canopy has a complex porous structure that is unevenly distributed and asymmetric is further supported by the discrepancy in the positioning data.

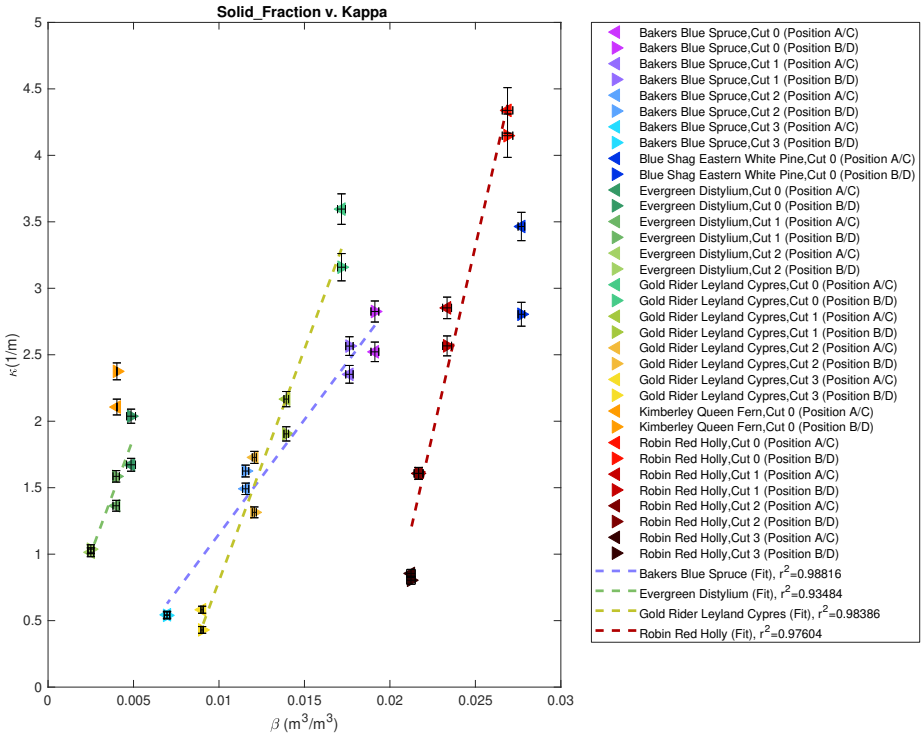

Fig. 10. Calculated absorption coeficients ($\varkappa$) plotted against their corresponding solid fractions (β)

4. Comparison Between Vegetation Data and Tube Bank Models

A hydraulic resistant tube bank model was evaluated using similar geometric features (absorption coefficient and solid fraction) of the vegetation canopy samples to compare the drag coefficients of the two different configurations. Given the absorption coefficient and solid fraction an optimization code was applied to determine the tube bank configuration. The absorption coefficient and solid fraction values were slightly adjusted to accomodate row and number of tube integers. Once a tube bank configuration was obtained, the pressure loss across the tube banks were determined using I.E. Idelchik's hydraulic resistant tube bank model. Eq. 3, was then evaluated given the adjusted tube bank configuration parameters to determine the drag coefficient. It should be noted that in the calculation for the tube bank's drag coefficient, the distance L was assumed to be between rows alternative to across the entire vegetation.

Acknowledgments

Matthew Bundy and Artur Chernovksy of the National Fire Research Laboratory assisted in conducting these experiments and in processing the data.

References

[1] Institute II (2018) Facts+Statistic: Wildfires, . URL https://www.iii.org/fact-statistic/facts-statistics-wildfires.

[2] Pimont F, Dupuy J, Linn RR, Dupont S (2009) Validation of firetec wind-flows over a canopy and a fuel-break. *Int J Wildland Fire* 18(7):775–790. https://doi.org/10.1071/WF07130

[3] Dupont S, Brunet Y (2008) Edge flow and canopy structure: a large-eddy simulation study. *Boundary Layer Meteorology* 126(1):51–71. https://doi.org/10.1007/s10546-007-9216-3

[4] E Mueller AS W Mell (2014) Large eddy simulation of forest canopy flow for wildland fire modeling. *Canadian J Forest Res* 44(12):1534–1544. https://doi.org/10.1139/cjfr-2014-0184

[5] J Cao AY Y Tamura (2012) Wind tunnel study on aerodynamic characteristics of shrubby specimens of three tree species. *Urban Forestry and Urban Greening* 11(4):465–476. https://doi.org/10.1016/j.ufug.2012.05.003

[6] J Jalonen JJ (2014) Estimation of drag forces caused by natural woody vegetation of different scales*. *J Hydrodynamics* 26(4):608–623. https://doi.org/10.1016/S1001-6058(14)60068-8

[7] Mayhead G (1973) Some drag coefficients for british forest trees derived from wind tunnel studies. *Agricultural Meterology* 12:123–130. https://doi.org/10.1016/0002-1571(73)90013-7

[8] Gillies JA (2002) Drag coefficient and plant form response to wind speed in three plantspecies: Burning bush (euonymus alatus), colorado blue spruce (picea pungens glauca.), and fountain grass (pennisetum setaceum). *J Geophysical Research* 107(D24):ACL 10–1–ACL 10–15. https://doi.org/10.1029/2001JD001259

[9] H Ishikawa YK A Suguru Amano (2006) Flow around a living tree. *JSME International Journal Series B Fluids and Thermal Engineering* 49(4):1064–1069. https://doi.org/10.1299/jsmeb.49.1064